Magnetostatic-Forward-Volume-Wave-Based Guided-Wave Magneto-Optic Bragg Cells and Applications to Communications and Signal Processing

CHEN S. TSAI, FELLOW, IEEE, AND DAVID YOUNG, STUDENT MEMBER, IEEE

Abstract—**In this paper realization of magnetostatic forward volume wave (MSFVW) based guided-wave magneto-optic (MO) Bragg cells and their applications to communications and signal processings are reported. First, Bragg diffraction of guided optical waves from the MSFVW in a noncollinear coplanar geometry is analyzed. The design of microstrip line transducers that facilitate wide-band MO Bragg diffraction with electronically tunable microwave carrier frequencies (2.0 to 12.0 GHz) is then briefly discussed. Subsequently, the experimental results obtained with the resulting Bragg cells in both pure and bismuth-doped YIG waveguides and a comparison to the theoretical predictions are presented. Finally, applications of the MO Bragg cells to light beam modulation, scanning/switching, and RF spectral analysis are presented in detail.**

I. INTRODUCTION

MAGNETO-OPTICS in waveguide structures [1]–[3], especially in those made of garnet films, was among the subject areas actively pursued during the early phase of research in guided-wave optics. A revival of interest in this subject area has taken place since. For example, various nonreciprocal guided-wave magneto-optic (MO) devices, e.g., the isolators and mode converters using yttrium iron garnet–gadolinium gallium garnet (YIG-GGG) waveguides [1], [2], have been proposed and demonstrated [3]–[12].

In the meantime, a variety of linear (low-power) and nonlinear (high-power) microwave devices [13], [14] that utilize magnetostatic waves (MSW's) in epitaxially grown YIG films on GGG substrates are currently going through engineering development. The maturity in the technology for excitation of the MSW's together with that for guided optical waves (GOW's) in the same substrate has also facilitated various studies on the interactions between the GOW's and the MSW's, and the resulting guided-wave MO devices [15]–[25]. The situation is similar to the research activity on the interactions between the GOW's and the surface acoustic waves (SAW's), and the resulting guided-wave acousto-optic (AO) devices in the mid 1970's [26].

Manuscript received July 28, 1989; revised December 18, 1989

The authors are with the Department of Electrical and Computer Engineering and the Institute for Surface and Interface Science, University of California, Irvine, CA 92717.

IEEE Log Number 8934043.

Similar to the guided-wave AO interactions in which the SAW induces a moving optical grating through the photoelastic effect [26], the guided-wave MO interactions result from the moving optical grating induced by the MSW's through the Faraday and Cotton–Mouton effects [16]–[18]. Of particular interest to us is a noncollinear coplanar geometry of the type shown in Fig. 1, in which a portion of an incident guided lightwave is Bragg-diffracted and mode-converted (TE to TM mode and vice versa). The Bragg-diffracted light is scanned in the waveguide plane as the frequency of the MSW is tuned. We had earlier obtained a bandwidth of 480 MHz in such an interaction geometry with magnetostatic surface waves (MSSW's) in a pure YIG waveguide using a single microstrip line transducer together with a fixed homogeneous dc magnetic field [16]–[18]. As in the AO Bragg diffraction, in which the resulting modulator is called the AO Bragg cell, the resulting MO modulator is called the MO Bragg cell [27], [28].

We have recently obtained a very large bandwidth using the same interaction geometry with magnetostatic forward volume waves (MSFVW's) in a pure YIG waveguide, again using a single microstrip line transducer together with a fixed homogeneous dc magnetic field [27]. For example, a 3 dB bandwidth of 1.03 GHz with the tunable carrier frequency centered at 6.0 GHz was obtained at the optical wavelength of 1.317 μm. We have also used the resulting wide-band MO Bragg cells to perform light beam deflection and RF spectral analysis, and have obtained large numbers of deflected light spots and RF spectral analysis [28]. In a continuing effort we have most recently succeeded in the realization of X-band MO Bragg cells of superior performances in bismuth-doped YIG waveguides.

The purposes of this paper are to present new results and to provide a more detailed account of some of those reported most recently. First, Bragg diffraction of guided optical waves from the MSFVW with noncollinear coplanar geometry in YIG–GGG substrate is analyzed. The design of the microstrip line transducers that facilitate realization of wide-band MO Bragg cells with electronically tunable center frequencies (from 2.0 to over 12.0 GHz) is then briefly discussed. The detailed results ob-

0018-9480/90/0500-0560$01.00

tained with the experiments on MO Bragg diffraction in both pure and bismuth-doped YIG waveguides and a comparison to the theoretical predictions are presented subsequently. Finally, applications of the resulting Bragg cells to light beam modulation, scanning/switching, and RF spectral analysis are presented and discussed.

II. Theoretical Analysis of Noncollinear Coplanar Guided-Wave Magneto-Optic Bragg Diffraction

Fig. 1 shows the noncollinear coplanar interaction configuration to be analyzed. An incident lightwave of either TM_0 mode or TE_0 mode is to propagate in the planar (slab) YIG–GGG waveguide along the X axis. A dc magnetic field H_0 is applied in the Z axis to saturate the sample and a single-element microstrip line is used to excite the Y-propagating MSFVW. In the following a coupled-mode analysis similar to the one which we previously developed in conjunction with noncollinear coplanar MO interaction with MSSW's [29] is presented. The RF magnetizations m_x and m_y of the Y-propagating MSFVW are given by

$$m_x = |m_x|\cos(\Omega t - \vec{K}\cdot\vec{r}) = \frac{1}{2}|m_x|\left[e^{i(\Omega t-\vec{K}\cdot\vec{r})} + e^{-i(\Omega t-\vec{K}\cdot\vec{r})}\right] \tag{1a}$$

$$m_y = |m_y|\sin(\Omega t - \vec{K}\cdot\vec{r}) = \frac{1}{2i}|m_y|\left[e^{i(\Omega t-\vec{K}\cdot\vec{r})} - e^{-i(\Omega t-\vec{K}\cdot\vec{r})}\right] \tag{1b}$$

where the amplitudes $|m_x|$ and $|m_y|$ are assumed to be significantly smaller than M_0, and Ω and $\vec{K}$ designate, respectively, the radian frequency and the wave vector of the MSFVW. Finally, $\vec{r}$ denotes the position vector. The total changes in the permittivity tensor, $\Delta\overleftrightarrow{\epsilon}$, induced by the RF magnetizations of the MSFVW and the saturation magnetization M_0 via the Faraday and the Cotton–Mouton effects are given as follows:

$$\Delta\overleftrightarrow{\epsilon} = \epsilon_0\begin{bmatrix} 0 & if_1M_0 & -if_1m_y \\ -if_1M_0 & 0 & if_1m_x \\ if_1m_y & -if_1m_x & 0 \end{bmatrix} \quad \text{(dynamic Faraday effect)}$$

$$+\epsilon_0\begin{bmatrix} \left(f_{12}+\frac{1}{3}\Delta f\right)M_0^2 & 0 & 0 \\ 0 & \left(f_{12}+\frac{1}{3}\Delta f\right)M_0^2 & 0 \\ 0 & 0 & \left(f_{12}+2f_{44}+\frac{1}{3}\Delta f\right)M_0^2 \end{bmatrix} \quad \text{(static Cotton–Mouton effect)}$$

$$+\epsilon_0\begin{bmatrix} -\frac{\sqrt{2}}{3}\Delta fM_0m_x & \frac{\sqrt{2}}{3}\Delta fM_0m_y & \left(2f_{44}+\frac{2}{3}\Delta f\right)M_0m_x \\ \frac{\sqrt{2}}{3}\Delta fM_0m_y & \frac{\sqrt{2}}{3}\Delta fM_0m_x & \left(2f_{44}+\frac{2}{3}\Delta f\right)M_0m_y \\ \left(2f_{44}+\frac{2}{3}\Delta f\right)M_0m_x & \left(2f_{44}+\frac{2}{3}\Delta f\right)M_0m_y & 0 \end{bmatrix} \quad \text{(dynamic Cotton–Mouton effect)} \tag{2}$$

where f_{11}, f_{12}, and f_{44} are the three independent components of the linear or second-order magnetic birefringence (Cotton–Mouton effect) in which $\Delta f \equiv f_{11} - f_{12} - 2f_{44}$; f_1 is the circular or first-order magnetic birefringence (Faraday effect) and is approximately equal to $2\sqrt{\epsilon_r}\phi_r/(k_0M_0)$ in which ϵ_r and ϕ_r are, respectively, the relative permittivity and the Faraday rotation of the YIG film, and $k_0 = (2\pi/\lambda_0)$ is the wavenumber of the lightwave in which λ_0 is the light wavelength in free space; ϵ_0 is the permittivity of free space; and i designates the imaginary number.

It is seen from (2) that both the dynamic Faraday effect and the dynamic Cotton–Mouton effect will cause coupling between the undiffracted (incident) light in the TM_0 mode and the diffracted light in the TE_0 mode, and vice versa. Since the uniaxial anisotropy induced by the static Cotton–Mouton effect can be directly incorporated in the calculation for the TE and TM normal modes of the YIG–GGG waveguide, only the dynamic effects induced by the MSFVW are to be considered in the following analysis. Thus, the second term of (2) is omitted henceforth. Furthermore, only the dominant transverse electric field component of the TM_0 mode is considered together with the transverse electric field of the TE_0 mode. It should be noted, however, that the coupling effect from the weaker longitudinal electric field component of the TM modes can also become significant in specially designed multilayer magneto-optic waveguide structures [30].

We shall derive in the following the coupled-mode equations for TM_0-mode incident light being Bragg-scattered at small angles by the MSFVW. The transverse electric field component of the TM_0-mode undiffracted light, E_z, and that of the TE_0-mode diffracted light, E_y, can be written as follows:

$$E_z(x,y,z) = \frac{1}{2}A(x)\,\varepsilon_z(z)\,e^{i[\omega_u t - \vec{\beta}^{(u)}_{TM_0}\cdot\vec{r}]} + \text{C.C.} \tag{3a}$$

$$E_y(x,y,z) = \frac{1}{2}D(x)\,\varepsilon_y(z)\,e^{i[\omega_d t - \vec{\beta}^{(d)}_{TE_0}\cdot\vec{r}]} + \text{C.C.} \tag{3b}$$

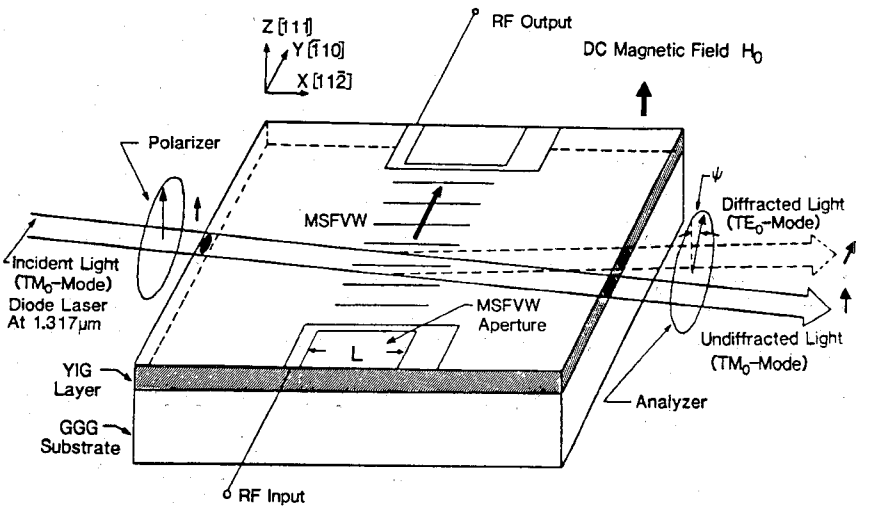

Fig. 1. Noncollinear coplanar interaction between guided optical waves and magnetostatic forward volume waves (MSFVW's) in YIG–GGG waveguide.

Here $A(x)$ denotes the complex amplitude of the *undiffracted* light with wave vector $\vec{\beta}^{(u)}_{TM_0}$ and angular frequency ω_u, and $D(x)$ is the complex amplitude of the *diffracted* light with wave vector $\vec{\beta}^{(d)}_{TE_0}$ and angular frequency ω_d. The quantities $\epsilon_z(z)$ and $\epsilon_y(z)$ are, respectively, the normalized transverse functions of the TM_0 and the TE_0 modes of the waveguide. The wave equation under perturbation by the MSFVW's can be written as follows:

$$\nabla^2\vec{E} - \mu\epsilon\frac{\partial^2}{\partial t^2}\vec{E} = \mu\frac{\partial^2}{\partial t^2}\Delta\vec{\epsilon}\cdot\vec{E} \tag{4}$$

where μ is the permeability and $\epsilon = \epsilon_r\epsilon_0$ is the unperturbed permittivity. After substituting (1a), (1b), (3a), and (3b) into (4) and utilizing the orthonormal properties of the normal modes of a well-confined slab waveguide [31], and the approximations given by (5a) and (5b) in all slow varying (phase insensitive) terms,

$$\beta^{(d)}_{TE_0} \approx \beta^{(u)}_{TM_0} = k_0\sqrt{\epsilon_r} \tag{5a}$$

$$\omega_d = \omega_u \pm \Omega \approx \omega_u \tag{5b}$$

the following coupled-mode equations [32] that relate the diffracted light and the undiffracted light for the case involving a TM_0-mode incident light are obtained:

$$\frac{d}{dx}\begin{bmatrix} A^{\pm}(x) \\ D^{\pm}(x)\end{bmatrix} = \begin{bmatrix} 0 & -(\kappa_1 \mp \kappa_2)\exp(+i\Delta x) \\ (\kappa_1 \mp \kappa_2)\exp(-i\Delta x) & 0\end{bmatrix}\begin{bmatrix} A^{\pm}(x) \\ D^{\pm}(x)\end{bmatrix}. \tag{6}$$

Also, the following coupling coefficients κ_1 and κ_2 are identified:

$$\kappa_1 = \frac{k_0|m_x|}{4\sqrt{\epsilon_r}}(f_1) \qquad \text{(dynamic Faraday coupling coefficient)} \tag{7a}$$

$$\kappa_2 = \frac{k_0 M_0|m_y|}{4\sqrt{\epsilon_r}}\left(2f_{44} + \frac{2}{3}\Delta f\right) \qquad \text{(dynamic Cotton–Mouton coupling coefficient)} \tag{7b}$$

where $A^{\pm}(x)$ and $D^{\pm}(x)$ designate, respectively, the complex amplitudes of the TM_0-mode undiffracted and the TE_0-mode diffracted light. The + and − superscript signs designate, respectively, the situations for anti-Stokes (with frequency up-shifted diffracted light) and Stokes (with frequency down-shifted diffracted light) interactions. The following phase-matching condition and frequency relationship [32] have been imposed in arriving at (6):

$$\Delta \equiv \left|\vec{\beta}^{(d)}_{TE_0} - \vec{\beta}^{(u)}_{TM_0} \mp \vec{K}\right| \tag{8a}$$

$$\omega_d = \omega_u \pm \Omega \tag{8b}$$

where Δ designates the mismatch between the three wave vectors $\vec{\beta}^{(u)}_{TM_0}$, $\vec{\beta}^{(d)}_{TE_0}$, and $\vec{K}$. As indicated previously, due to the static Cotton–Mouton effect, the wavenumbers $|\vec{\beta}^{(u)}_{TM_0}|$ and $|\vec{\beta}^{(d)}_{TE_0}|$ differ by a small amount from those in the paramagnetic state (i.e., $4\pi M_0 = 0$). For the other case involving a TE_0-mode incident light, the corresponding coupled-mode equations are obtained from (6) by replacing $A^{\pm}$ with $D^{\mp}$, and $D^{\pm}$ with $A^{\mp}$, where $A^{\mp}(x)$ and $D^{\mp}(x)$ designate, respectively, the complex amplitudes of the TE_0-mode undiffracted and the TM_0-mode diffracted light. The corresponding phase-matching condition is obtained by replacing $\vec{\beta}^{(u)}_{TM_0}$ with $\vec{\beta}^{(u)}_{TE_0}$, and $\vec{\beta}^{(d)}_{TE_0}$ with $\vec{\beta}^{(d)}_{TM_0}$ in (8a).

For a pure YIG film such as the one used in our earlier work the following data are available [33]: $4\pi M_0 = 1750$ G, $\sqrt{\epsilon_r} = 2.2$, $\lambda_0 = 1.3$ μm, $f_1 = 2.44\times10^{-6}$ G^{-1}, $f_{11} - f_{12} = 8.76\times10^{-9}$ G^{-2}, $f_{44} = 5.84\times10^{-9}$ G^{-2}, $\Delta f = -2.92\times10^{-9}$ G^{-2}, $4\pi|m_x| \approx 47$ G, and $4\pi|m_y| \approx 46$ G for the MSFVW power in the 155 mW range. Therefore, it is calculated that $\kappa_1 \approx 2.87°/\text{cm}$ and $\kappa_2 \approx 1.56°/\text{cm}$. As to the Bi-doped YIG film used in our experiment the following data are available: $4\pi M_0 = 1800$ G, $\sqrt{\epsilon_r} = 2.47$, $\lambda_0 = 1.3$

μm, $f_1 = -2.88\times10^{-5}$ G^{-1}, $f_{11} - f_{12} = 8.76\times10^{-9}$ G^{-2}, $f_{44} = 5.84\times10^{-9}$ G^{-2}, $\Delta f = -2.92\times10^{-9}$ G^{-2}, $4\pi|m_x| \approx$ 68 G, and $4\pi|m_y| \approx 68$ G for the MSFVW power in the 60 mW range. Therefore, it is calculated that $\kappa_1 \approx -43.68°/\text{cm}$ and $\kappa_2 \approx 2.11°/\text{cm}$.

Since for the pure YIG films κ_1 and κ_2 are both positive and comparable in value, (6) clearly shows that for the case with a TM_0-mode incident light the coupling between the undiffracted and the diffracted light in the Stokes interaction is much stronger than that in the anti-Stokes interaction. In contrast, for the case with the TE_0-mode incident light the coupling in the anti-Stokes interaction is much stronger than that in the Stokes interaction. The resulting asymmetry in diffracted light intensity was confirmed in the experiments to be presented in Section IV. It is to be noted that such asymmetrical diffraction in bulk-wave MO interaction was reported previously [34]–[36].

A. Mode-Conversion Efficiency

We now return to the case in which the incident light is of the TM_0 mode, i.e., $A^{\pm}(x=0) = A_0$ and $D^{\pm}(x=0) = 0$. The explicit solutions for the undiffracted TM_0-mode light, $A^{\pm}(x)$, and the diffracted TE_0-mode light, $D^{\pm}(x)$, are found as follows:

$$A^{\pm}(x) = A_0\left\{\cos(\alpha^{\pm}x) - i\left[\frac{\Delta}{2\alpha^{\pm}}\right]\sin(\alpha^{\pm}x)\right\}\exp\left(i\frac{1}{2}\Delta x\right) \tag{9a}$$

$$D^{\pm}(x) = A_0\left[\frac{\kappa^{\pm}}{\alpha^{\pm}}\right]\sin(\alpha^{\pm}x)\exp\left(-i\frac{1}{2}\Delta x\right) \tag{8b}$$

where

$$\kappa^{\pm} \equiv \kappa_1 \mp \kappa_2 \tag{9c}$$

$$(\alpha^{\pm})^2 \equiv (\kappa^{\pm})^2 + \left[\frac{\Delta}{2}\right]^2. \tag{9d}$$

Finally, the mode-conversion efficiency $\eta^{\pm}$, defined as the ratio of the diffracted light intensity (at the output $x = L$) to the incident light intensity (at the input $x = 0$) under perfect phase matching, is given as follows:

$$\eta^{\pm} = \sin^2(\kappa^{\pm}L). \tag{10}$$

From (10) we again see that both the dynamic Faraday effect and the dynamic Cotton–Mouton effect contribute to the mode conversion. Parts (a) and (b) of Fig. 2 show the calculated plots of the mode-conversion efficiencies η^+ and η^- versus the aperture of the MSFVW with κ^+ and κ^- as parameters together with experimental data for the pure YIG and the Bi-doped YIG waveguides, respectively. It is seen that for the former the mode-conversion efficiency in the Stokes interaction is much higher than that in the anti-Stokes interaction. However, for the latter the difference between the two efficiencies is much smaller.

B. Interaction Bandwidth

We now turn to the bandwidth inherent in the MO interaction involved. It is known that the range of the wavelength (Λ) for the MSFVW in the frequency range of interest is several orders of magnitude larger than that of the SAW's [26]. Accordingly, for a given aperture (L) the angular spread ($\approx \Lambda/L$) of the wave vector ($\vec{K}$) for the MSFVW is larger than that for the SAW by several orders of magnitude. Thus, the resulting MO Bragg bandwidth will also be larger than the resulting AO Bragg bandwidth by the same order of magnitude. For example, one of the MO experiments to be described later utilizes the MSFVW with an aperture of 8.8 mm at the frequency range of 2 to 7 GHz. The calculated plots in Fig. 3 show that the corresponding wavelengths for the MSFVW range from 1.86 mm to 45 μm [40], [41]. Thus, the angular spread of the wave vector ranges from 12° to 0.3°. This angular spread is clearly much larger than that with the SAW at the same range of frequencies. In short, this large angular

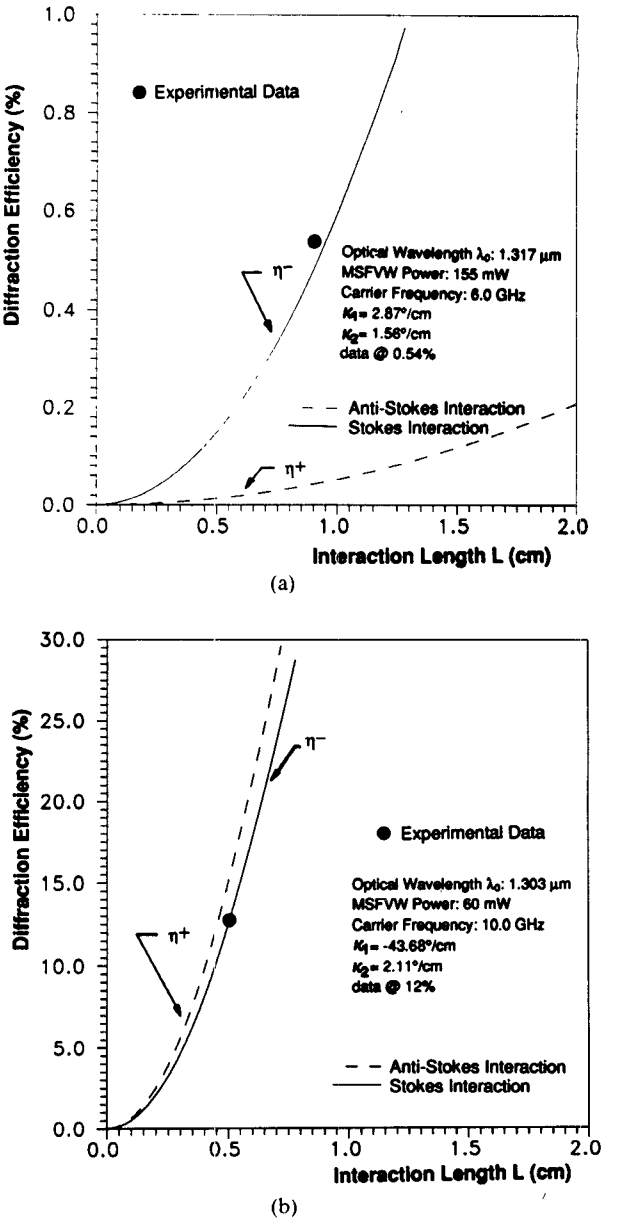

Fig. 2. (a) Diffraction efficiencies versus aperture of MSFVW for Stokes and anti-Stokes magneto-optic interactions in pure YIG waveguide. (b) Diffraction efficiencies versus aperture of MSFVW for Stokes and anti-Stokes magneto-optic interactions in Bi-doped YIG waveguide

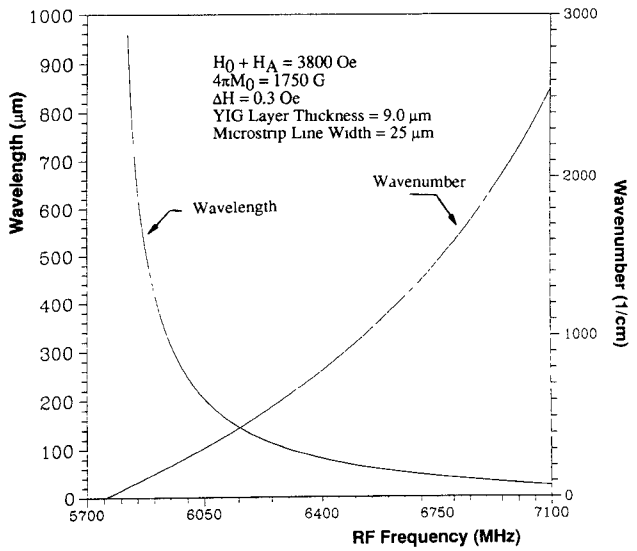

Fig. 3. Computer-generated wavenumbers and wavelengths of MSFVW in pure YIG waveguide.

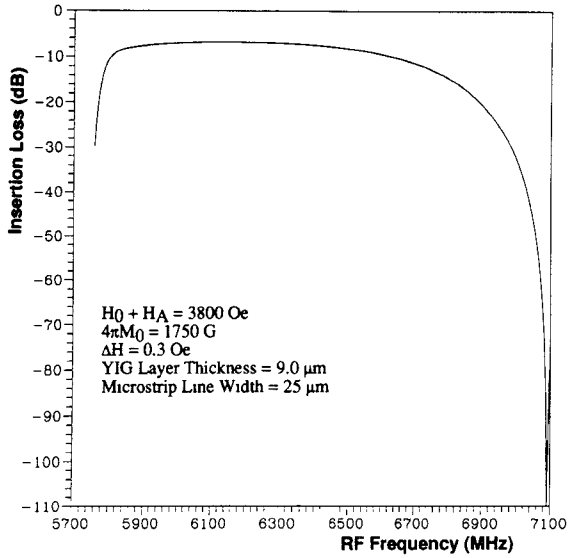

Fig. 4 Calculated frequency response of microstrip transducer insertion loss.

spread of the wave vector with the MSFVW facilitates wide-band phase matching and thus very large MO bandwidths that were measured in the experiments to be discussed in Section IV.

III. Design of Wide-Band Microstrip Line Transducer

The intrinsic bandwidth of the MSFVW, which is independent of the YIG film thickness and the transducer geometry, is given by the difference between the lower frequency limit f_L (at the wavenumber $K \to 0$) and the upper frequency limit f_U (at $K \to \infty$) of the dispersion relation [42]. For example, for pure YIG ($4\pi M_0 \approx 1750$ G and anisotropic field $H_A \approx 150$ Oe), this intrinsic bandwidth can be as large as 1.71 GHz at the operating frequency range of 2 GHz, and 2.2 and 2.36 GHz at the operating frequency of 10 and 30 GHz, respectively.

However, in order to capitalize on this large intrinsic bandwidth of the MSFVW, a transducer for its excitation must be properly designed. To date, the single-element shorted microstrip line transducer has demonstrated large bandwidth capability in MSW delay line applications. Moreover, thus far, only the single-element shorted microstrip line transducer can be modeled relatively accurately using computer simulations [43], [44]. Therefore, we have used computer simulation in the analysis and design of wide-band transducers of the shorted microstrip line type. Through computer simulation we have found the three key parameters that determine the ultimate bandwidth of the transducer for applications in MO Bragg diffraction: width of the microstrip line, thickness of the YIG layer, and ferromagnetic resonance (FMR) line width of the YIG layer. For example, Fig. 4 shows the frequency response of transducer insertion loss generated using computer simulation for the frequency range of 5.7 to 7.1 GHz for the set of geometrical and physical quantities that match the device that was used in one of the MO experiments to be presented in Section IV.

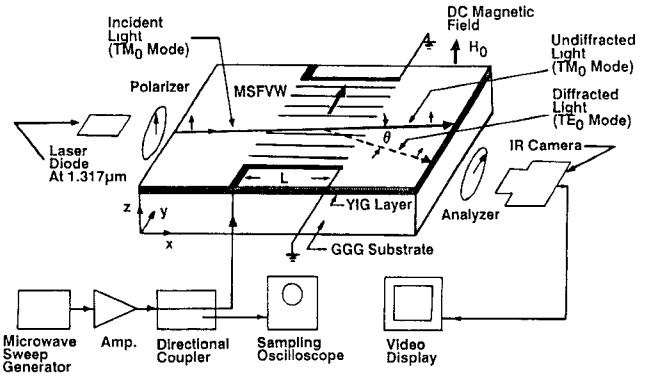

Fig. 5. Experimental arrangement for Bragg diffraction of guided light from MSFVW in YIG–GGG waveguide.

IV. Experiments on Magneto-Optic Bragg Diffraction

A number of measurements were carried out with both pure and Bi-doped YIG waveguides using the setup shown in Fig. 5. The YIG guiding layers were grown on the GGG substrate by liquid phase epitaxy. A light source at a wavelength of either 1.317 μm or 1.303 μm was edge-coupled into the YIG waveguide to excite either a TM_0-mode or a TE_0-mode guided light propagating in the X direction. The MSFVW was generated using a single-element shorted microstrip line transducer of proper width and length that was deposited on a quartz substrate and brought to near contact with the YIG waveguide. Efficient excitation of the MSFVW was accomplished over frequency bands by tuning a homogeneous dc magnetic field from 2000 to 4100 Oe. Appropriate beam-shaping optics was used to spatially separate the diffracted light from the undiffracted

light, and thus facilitate detailed measurements on mode-conversion (or diffraction) efficiency and bandwidth.

A. Pure YIG Waveguides

A 9-μm-thick YIG guided layer and a microstrip line 24 μm in width and 8.8 mm in length were used initially. As reported previously, a 3 dB bandwidth as large as 1.03 GHz centered at 6.0 GHz was obtained for a TM_0-mode incident light at a wavelength of 1.317 μm [27]. A 3 dB bandwidth of 0.78 GHz centered at 2.5 GHz was also measured with the same device. As indicated previously, these large bandwidths are in agreement with both the large calculated angular spreads of the wave vector of the MSFVW involved and the very large bandwidth of the microstrip line transducer used. These are by far the largest bandwidths that have been accomplished in guided-wave MO interactions.

The measured TM_0–TE_0 mode-conversion efficiencies for Stokes interaction are 0.54 and 0.50%, respectively, at the two center frequencies (6.0 and 2.35 GHz) under the RF drive power of 2.5 W. A linear dynamic range of about 12 dB was measured. The corresponding mode-conversion efficiencies for the anti-Stokes interactions were found to be much lower. As indicated in Fig. 2(a), the measured efficiency at 2.35 GHz (indicated in solid dot) is found to be in fair agreement with that predicted by the coupled-mode analysis. Slightly higher efficiencies were also measured in the experiments involving an incident lightwave of the TE_0 mode and the diffracted lightwave of the TM_0 mode.

B. Bismuth-Doped YIG Waveguides

The MO diffraction efficiency may be greatly improved by using Bi-doped YIG layers, as such materials possess much higher MO coefficients [45], [46] than the pure YIG layers. In the experiment, a cylindrical lens was used to focus a 100 mW collimated light beam from a 1.303 μm diode laser upon the Y–Z end face of the Bi-doped YIG-GGG substrate (furnished by Shin-Etsu Chemical Co. Ltd.) and excite a TE_0 mode propagating along the X axis. The refractive indices of the Bi-doped YIG and the doped GGG layers were measured directly using end-fire coupling to be 2.47 and 2.01, respectively. A Faraday rotation coefficient as large as $-2313°$/cm was measured. It is to be noted that this measured Faraday rotation coefficient is more than a tenfold increase over that of pure YIG layer [1], [2] and is in close agreement with that furnished by Shin-Etsu Chemical Co. Ltd., namely, $-2300°$/cm. As in the pure YIG waveguide, the Y-propagating MSFVW with an aperture of 5.0 mm would cause a coupling between the incident light of the TE_0 mode and the diffracted light of the TM_0 mode. However, since the magnitude of the Faraday rotation coefficient in the Bi-doped YIG layer was much larger than that of the Cotton–Mouton coefficient, the acute asymmetry in polarization-dependent diffraction between the Stokes and anti-Stokes diffracted beams in pure YIG waveguides [27] was no longer observed. Rather, diffracted beams of comparable intensity from both the Stokes and anti-Stokes directions were observed.

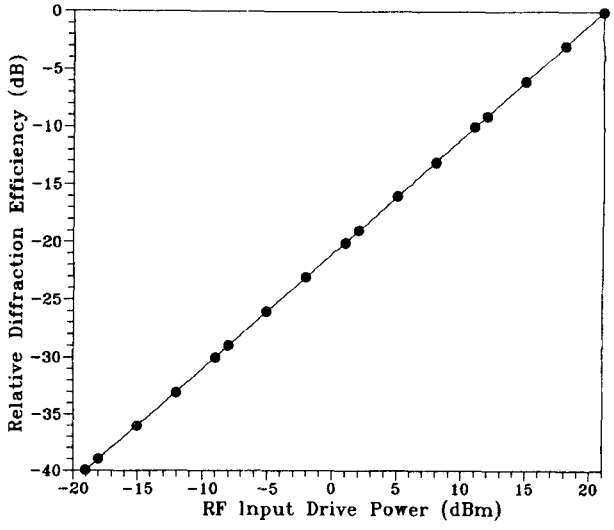

Fig. 6. Magneto-optic diffraction efficiency versus RF drive power at the carrier frequency of 10 GHz and dc magnetic field of 3660 Oe using Bi-doped YIG–GGG waveguide (YIG layer thickness = 3.9 μm).

Fig. 6 shows in dB the measured relative diffraction efficiency versus the RF drive power at the center frequency of 10.0 GHz. In this figure, the reference level (relative diffraction efficiency = 0 dB) corresponds to a diffraction efficiency of 0.84% measured at an RF drive power of 21 dBm (126 mW). A transducer conversion efficiency of -15.5 dB (or 2.8%) was measured. The return loss was measured to be -11 dB, indicating that most of the input drive power was used in generating the MSFVW. The measured diffraction efficiency was derived by using the following definition:

$$\text{diffraction efficiency (\%)} = \frac{\text{diffracted light intensity}}{\text{undiffracted (transmitted) light} + \text{diffracted light intensity}} \times 100.$$

Note that the total light intensity in the denominator is identical to the transmitted light at the output of the modulator when the RF drive power is off. It is seen that a linear dynamic range of 40 dB was accomplished. For RF drive power higher than 21 dBm, some deviation from linearity between the diffraction efficiency and the RF drive power was observed. However, a diffraction efficiency as high as 12% was measured at an RF drive power of 2 W (or a corresponding calculated MSFVW power of 56 mW based on the one-way transduction loss measurement). As shown in Fig. 2(b), the measured efficiency (indicated in solid dot) is in good agreement with the predicted value. The main causes of the transduction loss in a Bi-doped YIG MO Bragg cell include the microwave to MSFVW coupling loss, FMR line width loss, microstrip reactive loss, and exchange loss. The above diffraction efficiency and dynamic range represent, respectively, an improvement of 100 times and 28 dB over that previously obtained with the pure YIG Bragg cell of larger aperture (8.8 mm) at higher RF drive power (2.5 W), as described in

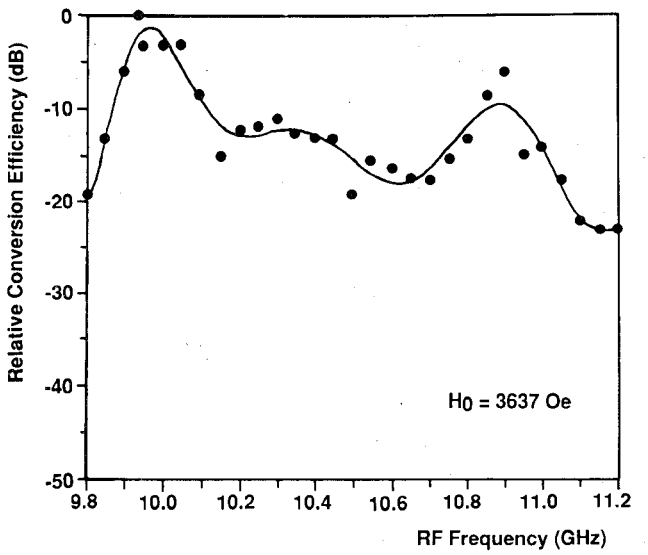

Fig. 7. Relative mode conversion efficiency versus the carrier frequency of MSFVW centered at 10.5 GHz for Bi-doped YIG MO Bragg cell.

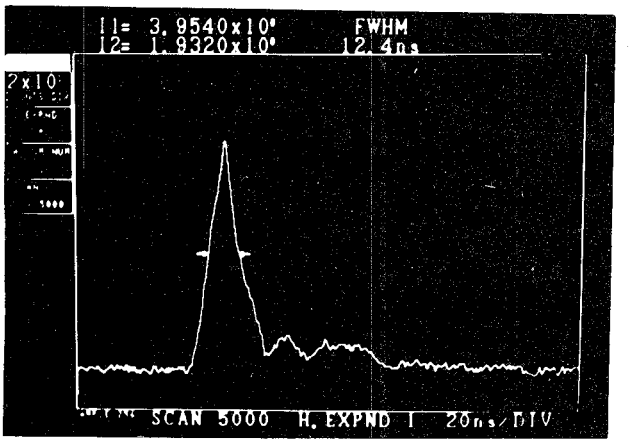

Fig. 8. Waveform of pulse-modulated guided light at 1.302 μm by Bi-doped YIG MO Bragg cell (carrier frequency of MSFVW = 10.5 GHz, H_0 = 3551 Oe, time scale = 20 ns per cm).

subsection IV-A. It is to be noted that the large increase in diffraction efficiency was a result of the large Faraday rotation coefficient associated with the Bi–YIG–GGG waveguides, and that the significant increase in dynamic range was also due to the relatively high output power of the laser diode. Comparable diffraction efficiency and linear dynamic range were measured by replacing the IR camera with a Ge photodetector as the center frequency of the MSFVW was tuned from 3.7 to 12.0 GHz, and the corresponding dc magnetic field was varied from 1430 to 4050 Oe. Finally, as shown in Fig. 7 at a fixed dc magnetic field of 3637 Oe, a 3 dB MO bandwidth of 150 MHz and a null-to-null MO bandwidth of 1.40 GHz were measured. These measured MO bandwidths are consistent with the calculated bandwidths of the microstrip line transducer employed. A significantly larger MO bandwidth should be achievable by careful tailoring of a single transducer or multiple transducers [10].

V. Applications of Guided-Wave Magneto-Optic Bragg Cells

The wide-band MO Bragg cells referred to above have been utilized to perform light beam modulation, scanning, and switching as well as RF spectral analysis. It should be noted that a number of studies on bulk-wave MO interactions involving unguided light waves and spin and/or magnetoelastic waves were reported in the late 1960's and early 1970's [34]–[39]. To the best of our knowledge, however, work neither on light beam deflection nor on RF spectral analysis using such bulk-wave MO interactions has been reported. A summary of the results obtained with such applications now follows:

A. Light Beam Modulation

By using the Bi-doped YIG MO Bragg cell, high-speed modulation of a guided light beam was demonstrated for the first time. In this experiment, a p-i-n switch that provided pulse modulation of the carrier at 10.5 GHz with approximately 10 ns rise time and 15 ns minimum pulse width was inserted between a microwave sweep generator and the input transducer of the MO Bragg cell. The aperture of the incident light beam was set at 0.5 mm. The diffracted light was then detected directly using a Hamamatsu 30 GHz optical sampling oscilloscope. Comparable rise times of 11 ns and 10.6 ns were measured, respectively, by using square-wave modulated pulses of 40 ns and 150 ns durations, as limited by the switching speed of the p-i-n switch. However, an optical pulse of triangular waveform as short as 12.4 ns (FWHM) was observed when a square-wave modulated pulse of 15 ns duration was used (Fig. 8). The modulated optical waveforms obtained correspond to the spatially integrated cross-correlation waveforms between the profile of the incident beam and the moving MO grating created by the pulse-modulated carrier at 10.5 GHz. Based on the group velocity of the MSFVW involved, a switching time of 15 ns has been calculated, which is, therefore, in good agreement with the experimental data. It should be noted that while the MO Bragg cells can provide a switching time faster than 10 ns per mm of the incident light beam aperture, the AO Bragg cells provide a much slower switching time, namely, on the order of 1 μs per mm of the incident light beam aperture.

B. Light Beam Scanning/Switching

Two types of light beam scanning experiments were carried out: one with the frequency of the MSFVW tuned continuously from the center frequency while keeping the dc magnetic field fixed, the other with the dc magnetic field tuned continuously while keeping the frequency of the MSFVW fixed. The photographs of the deflected light spots obtained with a pure YIG Bragg cell in the first experiment at the center frequency of 2.5 GHz, and in the second experiment with the frequency fixed at 2.2 GHz were presented earlier [28]. The photographs were taken from a video display through an IR camera. For the first experiment the diffracted light was scanned a total of 4° when the MSFVW frequency was tuned from 2.22 to 3.06

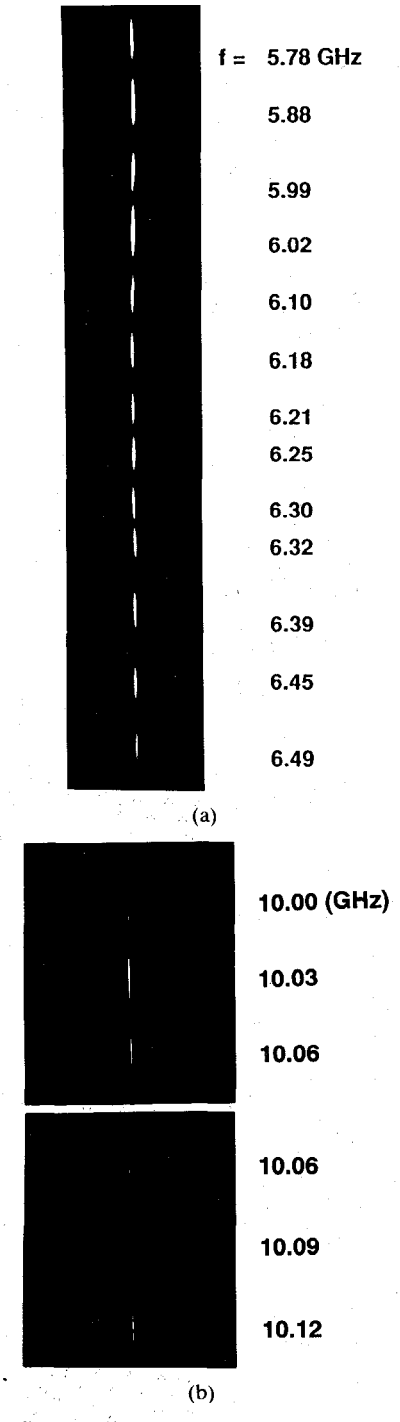

Fig. 9. (a) Deflected light spots obtained by varying the carrier frequency of MSFVW around 6 GHz using pure YIG MO Bragg cell. (b) Deflected light spots obtained by varying the carrier frequency of MSFVW around 10 GHz using bismuth-doped YIG MO Bragg cell.

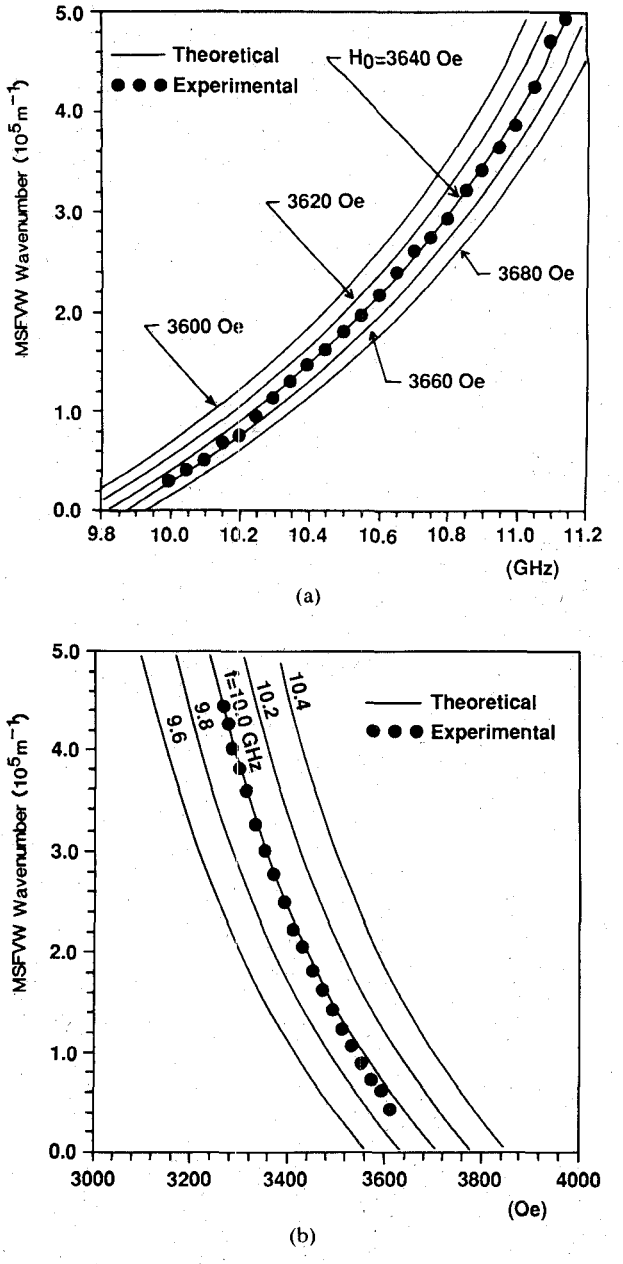

Fig. 10. (a) Calculated wavenumber of the MSFVW versus the carrier frequency with dc magnetic field as a parameter together with experimental data. (b) Calculated wavenumber of the MSFVW versus dc magnetic field with the carrier frequency as a parameter together with experimental data.

GHz. For the second experiment, the diffracted light was scanned a total of 2.7° when the dc magnetic field was tuned from 2175 to 1962 Oe. The dispersive (nonlinear) relationship between the frequency and the wavenumber of the MSFVW was also clearly demonstrated [28]. The diffracted light beam was scanned into more than 32 fully resolved spot positions in the first type of experiment and into more than 30 in the second type of experiment. Fig. 9(a) shows a series of deflected light spots obtained using the same pure YIG Bragg cell as the carrier frequency was varied from 6 GHz.

Fig. 9(b) shows a photograph of the deflected light spots obtained for an incident light 1.0 mm wide using the Bi-doped YIG Bragg cell by varying the carrier frequency around 10 GHz at a fixed dc magnetic field of 3660 Oe. The maximum measured angles of deflection for the diffracted light for the first and second types of experiment were 6° and 5.3°, respectively. Further measurements showed that the diffracted light beam was scanned over approximately 30 fully resolved spot positions in the first type of experiment and 27 in the second type of experiment. The wavenumber–frequency and wavenumber–dc magnetic field plots given in parts (a) and (b) of Fig. 10 show that the experimental data agree well with the calculated results.

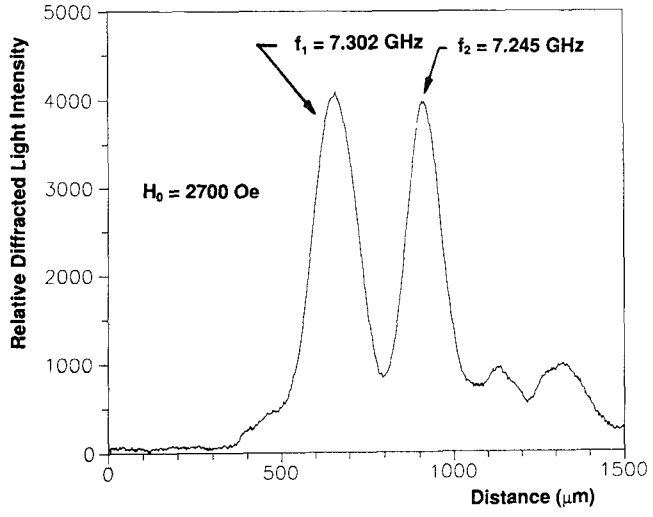

(a)

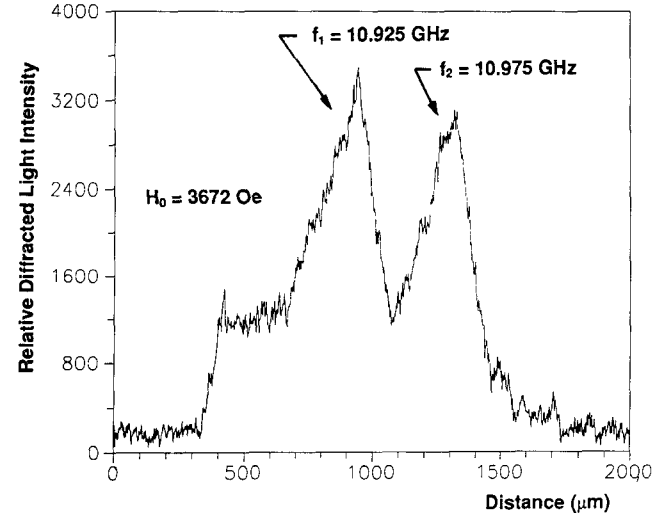

(b)

Fig. 11 (a) Deflected light beam scan plot for RF spectral analysis at 7.373 GHz using bismuth-doped YIG MO Bragg cell. (b) Deflected light beam scan plot for RF spectral analysis at 10.950 GHz using bismuth-doped YIG MO Bragg cell.

C. RF Spectral Analysis

As in guided-wave AO beam deflection, one of the potential applications of such wide-band MO beam deflection concerns real-time spectral analysis of wide-band RF signals [26], [28]. This application was readily demonstrated by simultaneously applying two RF signals of various frequency separation and power to the transducer of the Bi-doped YIG Bragg cells. Fig. 11(a) shows the profiles of two diffracted light spots obtained using the Beamscan Optical Profiler system (manufactured by Photon Inc.) instead of the IR camera as two carrier frequencies of 7.302 and 7.245 GHz were applied simultaneously. Similar results were obtained with the experiments performed at the center frequencies of 3.2 and 6.0 GHz. Finally, Fig. 11(b) shows the profiles of the two diffracted light spots obtained as two signals at 10.925 and 10.975 GHz were applied simultaneously to the Bi-doped YIG Bragg cell. Further measurements showed that a -1 dB frequency resolution of 30 MHz was achieved. By varying the relative power between the two signals by 10 dB, the diffracted light caused by the lower power signal could still be detected. Similar results were obtained at the carrier frequencies of 11.995 and 12.025 GHz. The measurable dynamic range was currently limited by the capability of the available hardware with the Beamscan Optical Profiler system. To the best of our knowledge, this experiment represents the highest frequency that has been used in RF spectral analysis using guided-wave optics. As mentioned in our earlier publications, MO Bragg cells with such high and tunable carrier frequencies permit direct processing at the carrier frequency and wide-band RF signals rather than indirect processing via frequency down-conversion, as is required with the AO Bragg cells. The latter necessarily results in more hardware and complexity in the receiver system, and thus higher cost.

VI. Conclusion

A number of significant advancements have been made in MSW-based guided-wave magneto-optics in recent years. These advancements include the growth of high-quality pure YIG-GGG waveguides; quality improvements in Bi-doped YIG-GGG waveguides; design and fabrication of efficient and wide-band transducers for the MSW's; theoretical analysis on noncollinear coplanar guided-wave MO interaction; construction of wide-band MO Bragg cells and demonstration of their applications in light beam modulation and scanning/switching and RF spectral analysis; fabrication of waveguide lens pairs; and the availability of high-field plate magnets. These advancements have paved the way for the realization of MSW-based integrated MO device modules such as high-speed optical scanners, multiport optical switches, and wide-band RF spectrum analyzers and correlators. Thus, the current status of development in the field is similar to guided-wave acousto-optics in the late 1970's. In comparison to their AO counterparts, the future MSW-based integrated MO device modules may possess the following unique advantages:

1) A much larger range of tunable carrier frequencies (2 to 20 GHz, for example) may be readily obtained by varying a dc magnetic field. Such high and tunable carrier frequencies with the MO device modules allow direct processing at the carrier frequency of wide-band RF signals rather than indirect processing via frequency down-conversion, as is required with the AO device modules.

2) A large MO bandwidth may be realized by means of a simpler transducer geometry.

3) Much higher and electronically tunable modulation/switching and scanning speeds are possible as the velocity of propagation for the MSW is higher than that of the SAW by one to three orders of magnitude, depending upon the dc magnetic field and the carrier frequency.

Acknowledgment

The authors wish to thank C. L. Wang, Y. Pu, and T. Q. Vu for technical assistance.

REFERENCES

[1] P. K. Tien and R. J. Martin, "Optical waveguides of crystal garnet films," *Appl. Phys. Lett.*, vol. 21, pp. 207–209, Sept. 1972.

[2] P. K. Tien, R. J. Martin, R. Wolfe, R. C. LeCraw, and S. L. Blank, "Switching and modulation of light in magneto-optic waveguides of garnet films," *Appl. Phys. Lett.*, vol. 21, pp. 394–396, 1972

[3] S. Wang, M. Shah, and J. D. Crow, "Studies of the use of gyrotropic and anisotropic materials for mode conversion in thin-film optical waveguide applications," *J. Appl. Phys.*, vol. 43, pp. 1861–1875, 1972.

[4] J. Warner, "Faraday optical isolator/gyrator design in planar dielectric waveguide form," *IEEE Trans. Microwave Theory Tech.*, vol. MTT-21, p. 769, 1973.

[5] S. C. Tseng, A. R. Reisinger, E. A. Giess, and C. G Powell, "Mode conversion in magneto-optic waveguides subjected to a periodic permalloy structure," *Appl Phys. Lett.*, vol. 24, pp. 265–267, 1974.

[6] S. Yamamoto, Y. Koyamada, and T. Makimoto, "Normal-mode analysis of anisotropic and gyrotropic thin-film waveguides for integrated optics," *J. Appl. Phys.*, vol. 43, pp. 5090–5097, 1972.

[7] G. Hepner, B. I. Désoimière, and J. P. Castéra, "Magnetooptic effects in garnet thin film waveguides," *Appl Opt.*, vol. 14, p. 1479, 1975.

[8] K. Ando, N. Takeda, T. Okuda, and N. Koshizuka, "Waveguide mode conversion by magnetic linear birefringence of Bi-substituted iron garnet films tilted from (111)," *J Appl. Phys.*, vol. 57, pp. 718–722, 1985.

[9] M. Torfeh, L. Courtois, L. Smoczynoki, H. LeGall, and J. M Desvignes, "Coupling and phase matching coefficients in a magneto-optical TE–TM mode converter," *Physica*, vol. 89B, pp. 255–259, 1977.

[10] R. Wolfe *et al.*, "Thin-film waveguide magneto-optic isolator," *Appl. Phys. Lett.*, vol. 46, pp. 817–819, May 1985.

[11] N. Koshizuka, K. Ando, and T. Okuda, "Growth-induced birefringence in LPE-grown iron garnet films," in *Proc. Int. Symp. Magneto-Optics, J. Magn. Soc. Jpn.*, vol. 11S, pp. 281–286, 1987.

[12] *Proc. Int. Symp. Magneto-Optics, J. Magn. Soc. Jpn.*, vol. 11S, 1987.

[13] J. M. Owens, R. L. Carter, C. V. Smith, Jr., and J. H. Collins, "Magnetostatic waves, microwave SAW?" in *1980 Ultrasonics Symp. Proc.*, 1980, pp. 506–513; also J. D. Adam, "Analog signal processing with microwave magnetics," *Proc. IEEE*, vol. 76, pp. 159–170, Feb. 1988.

[14] W. S. Ishak, "Magnetostatic wave technology: A review," *Proc. IEEE*, vol. 76, pp. 171–187, Feb. 1988.

[15] A. D. Fisher, J. N. Lee, E. S. Gaynor, and A. B. Tveten, "Optical guided-wave interactions with magnetostatic waves at microwave frequencies," *Appl. Phys. Lett.*, vol. 41, pp. 779–781, Nov. 1982.

[16] C. S. Tsai, "Hybrid integrated optic modules for real-time signal processing," in *Proc. NASA Opt. Inform. Process. Conf.* 1983, pp. 149–164.

[17] C. S. Tsai *et al.*, "Noncollinear coplanar magneto-optic interaction of guided optical wave and magnetostatic surface waves in yttrium iron garnet–gadolinium gallium garnet waveguides," *Appl. Phys Lett.*, vol. 47, pp. 651–654, Oct. 1985.

[18] C. S. Tsai, W. Chen, and D. Young, "Interaction between optical waves and magnetostatic surface waves in YIG–GGG waveguides," in *Proc. Int. Symp. Surface Waves in Solids and Layered Structures* (Novosibirsk, USSR), vol. III, July 1986, pp. 100–115

[19] H. Tamada, M. Kaneko, and T. Okamoto, "TM–TE optical-mode conversion induced by a transversely propagating magnetostatic wave in a $(BiLu)_3Fe_5O_{12}$ film," *J. Appl. Phys.*, vol. 64, pp. 554–559, July 1988.

[20] S. H. Talisa, "The collinar interaction between forward volume magnetostatic waves and guided light in YIG films," *IEEE Trans Magn.*, vol. 24, pp. 2811–2813, Nov. 1988.

[21] C. T. Wey, H. S. Tuan, J. P. Parekh, A. E. Craig, and J. N. Lee, "Enhanced-bandwidth MSFVW-optical interaction employing an inhomogeneous bias field," in *1986 Ultrason. Symp. Proc.*, pp. 173–178.

[22] H. H. He, Y. B. Li, and S. C. Zhou, "Optical mode conversion in a ferrimagnetic film containing a magnetostatic forward volume wave," in *1987 Intermag. Conf. Dig.* (Tokyo, Japan), Apr. 1987, paper: GC-10.

[23] A. N. Sigaev and A. A. Stashkevich, "Anisotropic diffraction of optical waveguide modes by a bulk spin wave in an yttrium iron garnet film," *Sov. Tech. Phys. Lett.*, vol. 14, pp. 209–210, Mar. 1988.

[24] O. G. Rutkin *et al.*, "Interaction of optical waveguide modes with spin waves in an yttrium iron garnet film," *Sov. Tech. Phys. Lett.*, vol. 11, pp. 386–387, Aug 1985.

[25] A. A. Sòlomko, Yu. A. Gaidai, A. V. Dovzhenko, M. V. Antonishin, and A. T. Yanishevskii, "Collinear interaction of light with surface magnetostatic waves in ferrite-garnet films," *Opt. Spectrosc. (USSR)*, vol. 61, pp. 804–807, Dec. 1986; also Yu. V. Gulyaev, I A. Ignat'ev, V. G. Plekhanov, and A F Popkov, "Waveguide propagation of light in a ferrimagnetic film containing a magnetostatic wave," *Sov Phys. Solid State*, vol. 27, pp. 845–847, May 1985.

[26] C. S. Tsai, "Guided-wave acoustooptic Bragg modulators for wide-band integrated optic communications and signal processing," *IEEE Trans. Circuits Syst.*, vol. CAS-26, pp. 1072–1098, 1979

[27] D. Young and C. S. Tsai, "GHz bandwidth magnetooptic interaction in YIG–GGG waveguide using magnetostatic forward volume waves," *Appl. Phys. Lett.*, vol. 53, pp. 1696–1698, Oct. 1988.

[28] C S. Tsai and D. Young, "Wideband scanning of guided-light beam and RF spectral analysis using magnetostatic forward volume waves in YIG–GGG waveguide," *Appl. Phys. Lett.*, vol. 54, pp. 196–198, Jan. 1989.

[29] C. S. Tsai, *et al.*, "Noncollinear coplanar magneto-optic interaction of guided optical wave and magnetostatic surface waves in yttrium iron garnet–gadolinium gallium garnet waveguides," *Appl. Phys. Lett.*, vol. 47, pp. 651–654, Oct. 1985.

[30] D. Marcuse, "Influence of position of magnetooptic layer on differential phase shift of slab waveguide," *IEEE J Quantum Electron.*, vol. QE-23, pp. 1268–1272, Aug. 1987.

[31] H. Kogelnik, "Theory of dielectric waveguides," in *Integrated Optics*, T. Tamir, Ed. New York: Springer–Verlag, 1979, ch. 2, pp. 13–81.

[32] A. Yariv, "Coupled-mode theory for guided-wave optics," *IEEE J. Quantum Electron.*, vol QE-9, pp. 919–933, Sept. 1973.

[33] R. V. Pisarev, I. G. Simi, N. N. Kolpakova, and Y. M. Yakovlev, "Magnetic birefringence of light in iron garnets," *Sov. Phys. JETP*, vol. 33, pp. 1175–1182, Dec. 1971.

[34] H. L. Hu and F. R. Morgenthaler, "Strong infrared-light scattering from coherent spin waves in yttrium iron garnet," *Appl. Phys. Lett.*, vol. 18, pp. 307–310, Apr. 1971.

[35] J H. Collins and D. A. Wilson, "Optical probing of magnetostatic modes in YIG delay lines," *Appl Phys Lett.*, vol. 12, pp. 331–333, 1968.

[36] B. Desormiere and H. LeGall, "Interaction studies of a laser light with spin wave and magnetoelastic waves propagating in a YIG bar," *IEEE Trans. Magn.*, (1972 INTERMAG Conf.), pp. 379–381, Sept. 1972.

[37] B. A. Auld and D. A. Wilson, "Spin and acoustic Bragg diffraction in longitudinal magnetoelastic waves," *Appl. Phys Lett.*, vol. 11, pp. 368–370, 1967.

[38] A. W. Smith, "Diffraction of light by magnetoelastic waves," *Appl. Phys. Lett.*, vol. 11, pp. 7–9, 1967.

[39] R. W. Dixon and H. Matthews, "Diffraction of light by elastic waves in YIG," *Appl. Phys. Lett.*, vol. 10, pp. 195–197, 1967.

[40] W. S. Ishak and K W. Chang, "Magnetostatic-wave devices for microwave signal processing," *Hewlett Packard J.*, vol. 36, pp. 10–20, Feb. 1985.

[41] I. J. Weinberg and J. C. Sethares, "Magnetostatic wave transducers with variable coupling," RADC In-House Report, RADC-TR-78-205, Sept 1978.

[42] R. W. Damon and H. Van De Vaart, "Propagation of magnetostatic spin waves at microwave frequencies in a normally-magnetized disk," *J. Appl. Phys.*, vol. 36, pp. 3453–3459, 1965.

[43] A. G. Ganguly and D. C. Webb, "Microstrip excitation of magnetostatic surface waves: Theory and Experiment," *IEEE Trans. Microwave Theory Tech.*, vol. MTT-23, pp. 998–1006, Dec. 1975

[44] P. R. Emtage, "Generation of magnetostatic surface waves by a microstrip," *J. Appl Phys.*, vol. 53, pp. 5122–5125, July 1982.

[45] H. LeGall, M Guillot, A. Marchand, Y. Nomi, and M. Artiman, "Faraday rotation in bismuth substituted iron garnets," in *Proc. Int. Symp. Magneto-Optics, J. Magn. Soc. Jpn.*, vol. 11S, pp. 235–240, Apr. 1987.

[46] J. P. Krumme, V Doormann, and R. Eckart, "Bismuth-substituted iron garnet films prepared by RF diode sputtering," *IEEE Trans. Magn.*, vol. MAG-20, pp. 983–985, Sept. 1984.

[47] H. Lenz, P. Hansen, and W. Tolksdorf, "Growth-induced magnetic and optic anisotropy in bismuth-substituted iron garnet films," *Appl. Phys. Lett.*, vol. 54, pp. 2484–2486, June 1989.

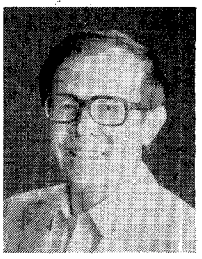

Chen S. Tsai (M'69–SM'77–F'83) is a naturalized citizen of the U.S. He received the Ph.D. degree in electrical engineering from Stanford University in 1965.

He was with the Lockheed Palo Alto Research Laboratories as a Research scientist for three and a half years before joining Carnegie-Mellon University as an Assistant Professor in 1969. In 1974 he was promoted to Professor of Electrical Engineering and was awarded an Endowed Chair Professorship in 1979. In the Fall of 1980 he joined the University of California at Irvine as a Professor of Electrical Engineering and served as Acting Department Chair from 1985 to 1986. The areas of his current research interest include integrated optics, guided-wave acousto-optics, electro-optics, magneto-optics, and acoustic microscopy. During the past 18 years, his group has carried various research projects in these areas. He has authored or coauthored some 180 research papers (42 invited), two of which won the IEEE Best Paper Award in Guided-Wave Acousto-Optics and Acoustic Microscopy, and six chapters in topical volumes, encyclopedias and handbooks. He currently serves as an Associate Editor of IEEE TRANSACTIONS ON ULTRASONICS, FERROELECTRONICS AND FREQUENCY CONTROL in the topical areas of optical interactions and acousto-optics. He is also the Editor-in-Chief of a Springer-Verlag volume on *Guided-Wave Acoustooptic Interactions, Devices, and Applications*, to which he has made pioneering and sustained contributions. He has organized and chaired several technical conferences and workshops on electro-optics, integrated optics, laser communications, and optical switching technology; has served on various technical program committees and chaired numerous technical sessions at national and international meetings.

Dr. Tsai is a Fellow of the Society for Photo Instrumentation Engineers, a Fellow of the Institute for the Advancement of Engineering, and a Fellow of the Optical Society of America. Included among his honors are the 1984 Outstanding Alumni Award from Utah State University, the 1985 U.C. Irvine Engineering Instructor of the Year Award, the 1986 U.C. Irvine Engineering Research Award, the 1986 IEEE Distinguished Lecturer Award of the Ultrasonics/Ferroelectrics/Frequency Control Society, and the 1987 Lauds/Laurels Award for Distinguished Research from the University of California at Irvine.

✠

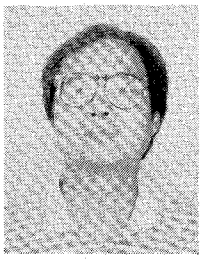

David Young (S'81) was born in Hong Kong on July 19, 1960. He received the B.Sc. degree in electrical and electronic engineering from University College, London, England, in 1981. Since 1983, he has been a research and teaching assistant in the Department of Electrical and Computer Engineering at the University of California, Irvine, where he obtained the M.S. and Ph.D. degrees in 1985 and 1989, respectively. His research interests are in the areas of integrated optics, magneto-optics, and magnetostatic waves devices.